UNIVERSITY OF BIRMINGHAM
University of Birmingham Research at Birmingham

Favorable residual stress induction by resin-cementation on dental porcelain

Fleming, Garry J P; Cao, Xu; Romanyk, Dan L; Addison, Owen

DOI:
10.1016/j.dental.2017.07.018

License:
Creative Commons: Attribution (CC BY)

Document Version
Publisher's PDF, also known as Version of record

Citation for published version (Harvard):
Fleming, GJP, Cao, X, Romanyk, DL & Addison, O 2017, 'Favorable residual stress induction by resin-cementation on dental porcelain', *Dental Materials*, vol. 33, no. 11, pp. 1258-1265. https://doi.org/10.1016/j.dental.2017.07.018

Link to publication on Research at Birmingham portal

General rights
Unless a licence is specified above, all rights (including copyright and moral rights) in this document are retained by the authors and/or the copyright holders. The express permission of the copyright holder must be obtained for any use of this material other than for purposes permitted by law.

•Users may freely distribute the URL that is used to identify this publication.
•Users may download and/or print one copy of the publication from the University of Birmingham research portal for the purpose of private study or non-commercial research.
•User may use extracts from the document in line with the concept of 'fair dealing' under the Copyright, Designs and Patents Act 1988 (?)
•Users may not further distribute the material nor use it for the purposes of commercial gain.

Where a licence is displayed above, please note the terms and conditions of the licence govern your use of this document.

When citing, please reference the published version.

Take down policy
While the University of Birmingham exercises care and attention in making items available there are rare occasions when an item has been uploaded in error or has been deemed to be commercially or otherwise sensitive.

If you believe that this is the case for this document, please contact UBIRA@lists.bham.ac.uk providing details and we will remove access to the work immediately and investigate.

Download date: 17. Apr. 2024

Available online at www.sciencedirect.com

ScienceDirect

journal homepage: www.intl.elsevierhealth.com/journals/dema

Favorable residual stress induction by resin-cementation on dental porcelain

Garry J.P. Fleming[a], Xu Cao[b], Dan L. Romanyk[c], Owen Addison[b,c,*]

[a] Materials Science Unit, Dublin Dental University Hospital, Lincoln Place, Trinity College Dublin, Dublin 2, Ireland
[b] Biomaterials Unit, University of Birmingham, School of Dentistry, 5 Mill Pool Way, Birmingham B5 7EG, UK
[c] University of Alberta, School of Dentistry, Edmonton, AB T6G 1C9, Canada

ARTICLE INFO

Article history:
Received 7 April 2017
Received in revised form
19 July 2017
Accepted 24 July 2017

Keywords:
Resin-cementation
Biaxial flexure strength
Shrinkage stress
Photo-polymerization
Fracture

ABSTRACT

Objectives. Despite developments in polycrystalline ceramics, glassy dental-ceramic materials provide the optimum cosmetic option in most clinical situations to mimic the natural dentition. The clinical success of glassy dental-ceramic materials is often attributed to resin-adhesive bonding techniques. In this study we explore whether shrinkage stresses generated on photo-polymerisation of the resin-cement are sufficient to induce ceramic surface defect stabilization, and we quantify the transient nature of the induced stresses.

Methods. Stress-induced changes in a feldspathic ceramic over a range of thicknesses (0.5–2.0 mm: n = 20 per thickness) were measured using a profilometric technique at baseline for each disc-shaped specimen (mean of the maximum deflection ($\delta_{baseline}$)) and again following polymerisation of a controlled resin-cement thickness on the contra-lateral surface. Measurements were repeated at 30, 60, 90 and 1440 min following photo-polymerization (δ_{30}, δ_{60}, δ_{90} and δ_{1440}, respectively) before bi-axial flexure strength (BFS) determination at 24 h.

Results. A repeated measures ANOVA and post-hoc Bonferroni tests determined that δ_{1440} was significantly different from $\delta_{baseline}$ ($p = 0.02$), δ_{30} ($p < 0.01$) and δ_{60} ($p < 0.01$) but not δ_{90} ($p = 0.61$). Data exploration revealed that there were differences in directionality of the independent variable (mean of the maximum deflection (δ)) with a proportion of specimens increasing in deflection and others reducing. The directionality of the effect strongly correlated with the BFS values. Where δ_{1440}-$\delta_{baseline}$ was low and/or negative, BFS values were also low. High BFS values were observed when δ_{1440}-$\delta_{baseline}$ was large and positive (indirectly inferring high shrinkage-stress-induced-deformation).

Significance. A link between shrinkage stresses associated with the photo-polymerization of dental resin-based cements and the reinforcement of dental porcelain has clearly been established.

© 2017 The Academy of Dental Materials. Published by Elsevier Ltd. This is an open access article under the CC BY license (http://creativecommons.org/licenses/by/4.0/).

1. Introduction

In 2002, a review entitled 'Are adhesive technologies needed to support ceramics? An assessment of the current evidence' concluded that resin-cements reinforce dental ceramics, however, the assessment of the 'available evidence' was poor [1]. Of the 28 studies reviewed [1], only two were direct clinical comparisons [2,3] with the remainder based on supposition, inconclusive *in vitro* mechanical tests including load-to-failure studies of adhesively cemented, anatomically

* *Corresponding author at*: Biomaterials Unit, University of Birmingham, School of Dentistry, 5 Mill Pool Way, Birmingham B5 7EG, UK.
E-mail addresses: o.addison@bham.ac.uk, oaddison@ualberta.ca (O. Addison).

http://dx.doi.org/10.1016/j.dental.2017.07.018

0109-5641/© 2017 The Academy of Dental Materials. Published by Elsevier Ltd. This is an open access article under the CC BY license (http://creativecommons.org/licenses/by/4.0/).

representative restorations. Unfortunately, the dental literature is replete with 'crunch-the-crown' load-to-failure studies [4–8] despite fracture behavior in such tests being dominated by the indenter-contact surface which fails to simulate clinical failure modes [9]. Load-to-failure studies of anatomically representative restorations add little to the mechanistic understanding of resin-cement strengthening and cannot be used to guide materials-development or inform the profession [10,11]. From the results of the two direct clinical comparison studies [2,3], it has become accepted that adhesive cementation of monolithic dental-ceramic restorations fabricated from glassy/glass-ceramic substrates is essential to optimise restoration longevity. When adhesively coupled to the underlying tooth substrate, relatively 'weak' ceramic materials demonstrate significantly higher clinical survival rates compared with acid-base cement systems [2,3]. This consensus was predicted by John McLean who postulated that the tooth could act as a 'reinforcing core' for ceramic restorations with the adhesive resin-cement providing a 'synergistic bond' to confer system strength [12]. Despite the mechanical advantages of polycrystalline ceramics [13], glassy ceramics still provide the optimum minimally invasive cosmetic option for the clinician to mimic tooth structure in terms of form, shade, translucency, lustre and hue [3]. It is for this reason that most polycrystalline ceramics have to 'veneer' the core material with porcelain which has subsequently become the mechanical 'weak-link' [13]. Extrapolating from McLean's postulation, two questions arise: (1) are we close to optimising the 'synergism' between the ceramic/resin-cement/tooth substrate complex? and (2) with appropriate technological development could reinforcing ceramic cores be eliminated completely from the prosthodontists armamentarium to herald a truly conservative all-ceramic indirect restoration?

To date, the way in which resin-cements reinforce ceramics remains poorly understood and studying the discrete components or model analogues of the ceramic/resin-cement/tooth substrate complex, in isolation and/or in combination, has been shown to be a useful *in vitro* approach [14–18]. When considering the fracture resistance of glass bonded to a relatively compliant polymer substrate, Lawn et al. [14] identified competing fracture modes, with fracture originating either from contact zone cone cracks during testing or from radial fracture at the glass-substrate interface. The observation of the former is encouraging as it demonstrates that it is possible to reinforce the glass sufficiently against radial failure so that contact damage failure predominates. Further studies have focused on the resin-cement/ceramic interface [19–21] and identified the magnitude of resin-strengthening is sensitive to the pre-existing ceramic surface defect population [19]. Different magnitudes of strengthening have been observed to be dependent on: the size of the critical ceramic surface defect [19]; the nature of bonding at the resin-cement/ceramic interface including silane coupling agents with pre-test storage (hydration and time) regime [20]; and the modulus of elasticity of the resin-cement [21].

One concept that has been minimally explored is whether resin-cementation of dental ceramic restorations confers compressive stabilisation of the 'fit' ceramic surface. In 1993, Nathanson suggested that the stresses generated due to the volumetric shrinkage associated with photo-polymerisation of methacrylate resin-based cements could exert a stabilising compressive stress over the surface flaw integral, thereby resulting in an increased energetic requirement to reach the critical tensile stress in the ceramic to initiate catastrophic failure [22]. The purpose of the current study was to first ascertain whether the shrinkage stresses generated on initial resin-cement photo-polymerisation are sufficient to confer surface defect stabilisation and secondly to understand the transient nature (or not) of the residual stresses conferred post photo-polymerisation of the resin-cement.

2. Materials and methods

2.1. *Specimen manufacture*

VITA VM7 (Vita Zahnfabrik, Bad Säckingen, Germany) disc-shaped specimens (13.8 mm nominal diameter) were fabricated by manipulating a porcelain slurry prepared to a powder/liquid mixing ratio of 0.3/0.11 g/mL of VM7 base dentin powder (Lot 7433)/modelling fluid (Lot 4209R) into Nylon ring-moulds (0.7, 1.2, 1.7 and 2.2 mm thicknesses: n = 20 per thickness) secured to a burnished aluminum baseplate [23]. The mould assembly was vibrated (Croform Techniques Ltd, London, UK) for 90 s and excess liquid was repeatedly removed using absorbent tissues [24]. Following condensation, surplus material was removed with a razor blade, and discs were sintered on a silicon-nitride firing-slab in a vacuum-furnace (Vita Vacumat 40, Vita Zahnfabrik, Bad Säckingen, Germany) which involved pre-heating to 500 °C for 420 s, before the temperature was increased at 55 °C/min to 910 °C under vacuum, held for 60 s and allowed to slow cool to room temperature (Vita VM7 Product Specification, 2016).

Both sides of the disc-shaped specimens were wet-polished for 90 s with increasing grades (from P320 to P600 and P800) of silicon carbide abrasive papers (Buehler, Lake Bluff, IL, USA) on an Alpha and Beta Grinder-Polisher (Buehler) at 100 rpm under a specimen force of 3.3 N, with an exchange of abrasive paper at 30 s time-intervals [25]. Specimen thicknesses were periodically measured with a digital micrometer (Digimatic Micrometer, Mitutoyo Corp., Tokyo, Japan) to create a distribution of disc-thicknesses ranging from 0.5 to 2.0 mm. The sintering of specimens at different material thicknesses (and therefore volumes) and the subsequent surface polishing introduces differences in residual stress state between individual disc-shaped specimens. To account for this, discs were annealed by heating from 200 to 610 °C in air at 20 °C/min, held at 610 °C for 40 min before cooling to 60 °C at 2.9 °C/min [26]. To create a surface conducive to profilometric evaluation of stress-induced-distortion in the disc-shaped specimens, one surface of each disc was further wet-polished with P1200, P2400 and P4000 abrasive papers under the conditions outlined above (100 rpm, at 3.3 N specimen force for 90 s time-intervals with abrasive paper exchange every 30 s). The contralateral surface of each disc-specimen was then air abraded with 50 μm diameter alumina particles from a distance of 1 cm, at a 90° angle of incidence and 2.5 bar pressure to produce a surface roughness conducive to bonding while imparting a consistent surface defect population [21]. The final disc-thicknesses were re-determined with the digital microm-

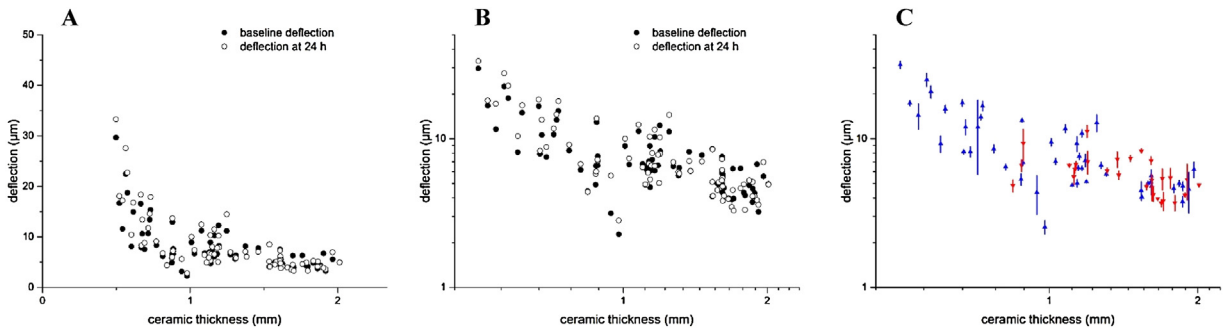

Fig. 1 – A) Scatter plot of mean of the maximum deflection before photo-polymerisation ($\delta_{baseline}$) and 24 h following photo-polymerisation (δ_{1440}) against ceramic disc-specimen thickness. B) Data shown on logarithmic axes demonstrating an approximate linear relationship between ln(deflection) and ln(ceramic thickness) at baseline and at 24 h. C) directional plot of data shown in 1B, demonstrating the vector of change between baseline deflection and 24 h deflection against ceramic thickness. Blue lines identify increases in deflection and red lines identify decreases in deflection after 24 h resin-coating. All data is shown (n = 80). (For interpretation of the references to colour in this figure legend, the reader is referred to the web version of this article.)

eter. Additionally, a further 20 disc-shaped specimens were fabricated using the 1.2 mm mould and finished to a 1 mm thickness using polishing regime outlined above while maintaining the identical annealing and air abrasion regimens employed to act as an un-cemented (control) group for bi-axial flexure strength (BFS) determination.

2.2. *Deflection determination*

The disc-shaped specimens were aligned on a three-axis levelling-device where a contact diamond stylus profilometer (Talysurf CLI 2000, Taylor-Hobson Precision, Leicester, UK) with a 90° conisphere stylus tip (2 μm radius) was used to perform 126 measurement traces across a 5 mm^2 area (10 mm length and 0.5 mm width) coincident with the center of the polished specimen surface. The area of interest (10 mm length and 0.5 mm width) was marked to ensure the consistency of subsequent repeat measurements [27]. Measurements were performed at a stylus velocity of 1 mm/s and an applied force of 0.75 mN, with a 4 μm step-size (y-direction), recording data points every 10 μm (x-direction) at a 40 nm resolution (z-direction). The mean of the maximum deflection (δ) was determined as the mean of the maximum central z-vector relative to the disc-periphery (μm) to provide an initial baseline (pre photo-polymerisation) measurement ($\delta_{baseline}$).

The alumina-particle-air-abraded surface of each disc-shaped specimen was primed with 3-methacryloxypropyltrimethoxysilane (Rely-X Ceramic Primer, 3 M ESPE) and allowed to air-dry (23 ± 1 °C at 50 ± 1% relative humidity) for 10 min. To standardise the cementation process and generate a consistent resin-cement thickness, 0.035 g of Rely-X Veneer Cement (3 M ESPE) was deposited onto the center of the primed-disc [25], covered with a thin acetate sheet and a 1 mm thick glass slide and pressed under a standard load until the resin-cement spread to the disc-periphery. The resin-cement was light-irradiated using an Optilux 501 light-curing-unit (SDS Kerr, Danbury, CT, USA) for 20 s at a light intensity of 740 ± 38 mW cm^{-2} with a 13 mm light-tip-diameter, held against the glass slide during photo-polymerisation. The thicknesses of the resin-cemented discs were determined at three separate points and the mean resin-cement thicknesses calculated. Repeat profilometric measurements were performed over the measurement track at 30, 60, 90 and 1440 min following photo-polymerisation (using the protocol employed above) to obtain the mean of the maximum deflection values (μm) namely δ_{30}, δ_{60}, δ_{90}, and δ_{1440}, respectively. All measurements were performed at room temperature of 23 ± 2 °C and a relative humidity of 50 ± 10%.

Immediately following the determination of δ_{1440}, the BFS (σ) of all disc-shaped specimens were determined using a ball-on-ring assembly where the resin-coated-discs were positioned centrally on a knife-edged-support (10 mm diameter) with the polished surface uppermost and loaded with a stainless-steel spherical ball-indenter (4 mm diameter) at 1 mm/min. σ was calculated at the disc-center at axial positions throughout the specimen thickness (z), with the bonded interface at z = 0, the ceramic surface at z = t_1 and the resin-surface at z = $-t_2$ using the approach described by Hsueh et al. [28].

$$\sigma = \frac{-3P(1+\nu)(z-t_n)}{2\pi(t_1+t_2)^3}\left[1+2\ln\left(\frac{a}{b}\right)+\frac{1-\nu}{1+\nu}\left(1-\frac{b^2}{2a^2}\right)\frac{a^2}{R^2}\right]\left[\frac{E_1{}^*(E_1{}^*t_1+E_2{}^*t_2)(t_1+t_2)^3}{\left(E_1{}^*t_1{}^2\right)^2+\left(E_2{}^*t_2{}^2\right)^2+2E_1{}^*E_2{}^*t_1t_2\left(2t_1{}^2+2t_2{}^2+3t_1t_2\right)}\right] \quad (1.1)$$

$(0 \le z \le t_1)$ and

$$\sigma = \frac{-3P(1+\nu)(z-t_n)}{2\pi(t_1+t_2)^3}\left[1+2\ln\left(\frac{a}{b}\right)+\frac{1-\nu}{1+\nu}\left(1-\frac{b^2}{2a^2}\right)\frac{a^2}{R^2}\right]\left[\frac{E_2{}^*(E_1{}^*t_1+E_2{}^*t_2)(t_1+t_2)^3}{\left(E_1{}^*t_1{}^2\right)^2+\left(E_2{}^*t_2{}^2\right)^2+2E_1{}^*E_2{}^*t_1t_2\left(2t_1{}^2+2t_2{}^2+3t_1t_2\right)}\right] \quad (1.2)$$

$(-t_2 \le z \le 0)$ and

$$\nu = \frac{(\nu_1 t_1+\nu_2 t_2)}{t_1+t_2} \quad (1.3)$$

Table 1 – Summary of relationships between variables. Pearson product-moment correlation coefficient generated to identify a relationship between the change in the maximum deflection 24 h following photo-polymerisation of the resin-cement [δ_{1440}-$\delta_{baseline}$] and BFS. Results of linear regression testing between mean of the maximum deflection 24 h following photo-polymerisation (δ_{1440}); baseline deflection ($\delta_{baseline}$), ceramic thickness (t_1); disc-flexural rigidity (D) and 24 h BFS value. Where relationships were clearly non-linear (Figs. 1–3), natural log transforms were performed.

Correlation		Significance	Pearson's coefficient (r)
Variable 1	Variable 2		
[δ_{1440}-$\delta_{baseline}$]	BFS	$p<0.001$	0.68
Linear Regression		**Significance**	**R^2-value**
Variable 1	Variable 2		
$\ln(t_1)$	$\ln[\delta_{baseline}]$	$p<0.001$	0.48
$\ln(t_1)$	$\ln[\delta_{1440}]$	$p<0.001$	0.59
ln(D)	[δ_{1440}-$\delta_{baseline}$]	$p=0.09$	0.16
$\ln(t_1)$	ln(BFS)	$p<0.001$	0.64

P was the load at fracture, ν_1 and ν_2 the Poisson's ratios of the VM7 ceramic (0.23 [29]) and Rely-X Veneer Cement (0.27 [30]), respectively. a, b and R were the radii of the knife-edge-support, loaded region and specimen, respectively. t_n was the neutral axis of bending calculated from the ceramic thickness (t_1), resin-cement thickness (t_2), elastic modulus of the ceramic ($E_1 = 66.7$ GPa [29]) and Rely-X Veneer Cement ($E_2 = 8.2$ GPa [30]) where

$$t_n = \frac{E_1^*(t_1)^2 - E_2^*(t_2)^2}{2(E_1^* t_1 + E_2^* t_2)} \quad (1.4)$$

$$E^* = \frac{E}{1-\nu^2} \quad (1.5)$$

To enable the correlation between σ or δ and the deformability of disc-shaped-specimens of different ceramic thicknesses, the flexural rigidity (D) of the discs were calculated from the plate constant for flat circular plates of constant thickness [31].

$$D = \frac{Et^3}{12(-\nu^2)} \quad (1.6)$$

2.3. *Statistical Analyses*

The baseline mean of the maximum deflection ($\delta_{baseline}$) value was compared with the following photo-polymerisation mean of the maximum deflections (δ_{30}, δ_{60}, δ_{90}, and δ_{1440}) using a repeated measure analysis of variance (ANOVA) for correlated samples and a Greenhouse-Geisser correction (accounting for violation of the assumption for sphericity) [32]. Post-hoc testing between different photo-polymerisation time-points was conducted using a Bonferroni correction ($\alpha = 0.05$.) Pearson product-moment correlation coefficients were generated to explore the correlation between independent variables, namely the change in deflection at 24 h following photo-polymerisation and BFS. Linear regression was performed to identify the nature of the relationships between mean of the maximum deflection or BFS, with ceramic thickness and flexural rigidity. All statistical tests were conducted at a significance level of $\alpha = 0.05$

3. Results

A repeated measures ANOVA determined that δ differed significantly ($p<0.001$) between the five time points employed (0 (baseline) and 30, 60, 90 and 1440 min following photo-polymerisation). Post-hoc tests revealed that the mean of the maximum deflection (δ_{1440}) was significantly different from $\delta_{baseline}$ ($p=0.02$), δ_{30} ($p<0.01$) and δ_{60} ($p<0.01$) but not δ_{90} ($p=0.61$). Data exploration revealed differences in directionality of the independent variable (mean of the maximum deflection (δ)) with a proportion of the disc-shaped specimens increasing in mean of the maximum deflection with others reducing (Fig. 1). The greatest initial mean of the maximum deflections at $\delta_{baseline}$ (before photo-polymerisation) were observed for 0.5 mm disc-thicknesses, decreasing exponentially with increasing ceramic thickness until a disc-thickness of ~1.0 mm, whereupon a mean of the maximum deflection ($\delta_{baseline}$) was maintained at ~5 μm (Fig. 1A). The data re-plotted on logarithmic axes identified an approximately linear relationship between ceramic thickness and $\delta_{baseline}$ or δ_{1440} (Fig. 1B, and results of regression analysis in Table 1).

Following resin-coating (mean resin-cement thickness 0.25 ± 0.08 mm) and 24 h photo-polymerization storage, δ_{1440} was observed to change with the greatest differences occurring for disc-shaped specimen thickness of <0.75 mm. Exploring the data further revealed that both the central z-vector relative to the disc-periphery and magnitude of change in the mean of the maximum deflection differed, with some specimens increasing (their central deflection) while others did not (Fig. 1C). A clear correlation between D and the vector of change in mean of the maximum deflection was observed with δ_{1440}-$\delta_{baseline}$ following an approximate exponential decay with increasing D values. Similarly, specimens with the lowest D values were more likely to increase the mean of the maximum deflection whilst specimens with higher D values had a tendency to flatten (not display an increase in the maximum deflection) when evaluated at 24 h post photo-polymerisation (Fig. 2).

The mean BFS value of the resin-cemented specimens tested 24 h following photo-polymerisation was 115 ± 35 MPa ranging from 62 to 230 MPa and was significantly increased when compared with the mean BFS (72 ± 9 MPa) of the

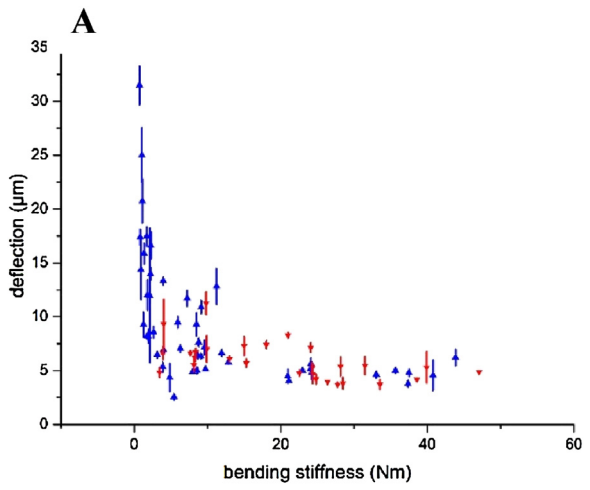

Fig. 2 – Vector plot of changes to the maximum deflection following photo-polymerisation at 24 h compared with baseline (before photo-polymerisation) against bending stiffness (disc-flexural rigidity). Blue lines identify increases in deflection and red lines identify decreases in deflection after 24 h resin-coating. All data shown (n = 80). (For interpretation of the references to colour in this figure legend, the reader is referred to the web version of this article.)

uncoated control group (Fig. 3A). Given the clear non-linear relationships between the mean of the maximum deflection 24 h following photo-polymerisation and ceramic thickness (δ_{1440} and t_1), disc-flexural rigidity and the difference in the mean of the maximum deflection values on photo-polymerisation (D and δ_{1440}-$\delta_{baseline}$), ceramic thickness and BFS value (t_1 and BFS), natural log transformations of the data were performed prior to regression analyses (Table 1).

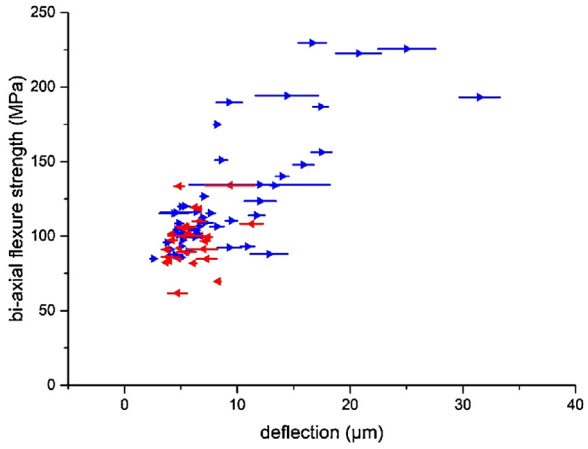

Fig. 4 – Vector plot of mean of the maximum deflection at 24 h following photo-polymerisation (δ_{1440}) against BFS values. Blue lines identify increases in deflection and red lines identify decreases in deflection at 24 h. All data shown (n = 80). (For interpretation of the references to colour in this figure legend, the reader is referred to the web version of this article.)

Finally, when considering the relationship between the difference in photo-polymerisation mean of the maximum deflection values (δ_{1440}-$\delta_{baseline}$) with BFS, a clear pattern arose. Test specimens where the magnitude of the change in mean of the maximum deflection (δ_{1440}-$\delta_{baseline}$) was low and/or negative were clustered at low BFS values exhibiting the least reinforcement (Fig. 4). Conversely, specimens with high BFS values demonstrated large and positive increases in magnitude of the change in mean of the maximum deflection (δ_{1440}-$\delta_{baseline}$). The Pearson correlation coefficient generated for δ_{1440}-$\delta_{baseline}$ and BFS was statistically significant, positive and strong ($r = 0.68$, $n = 80$, $p < 0.001$).

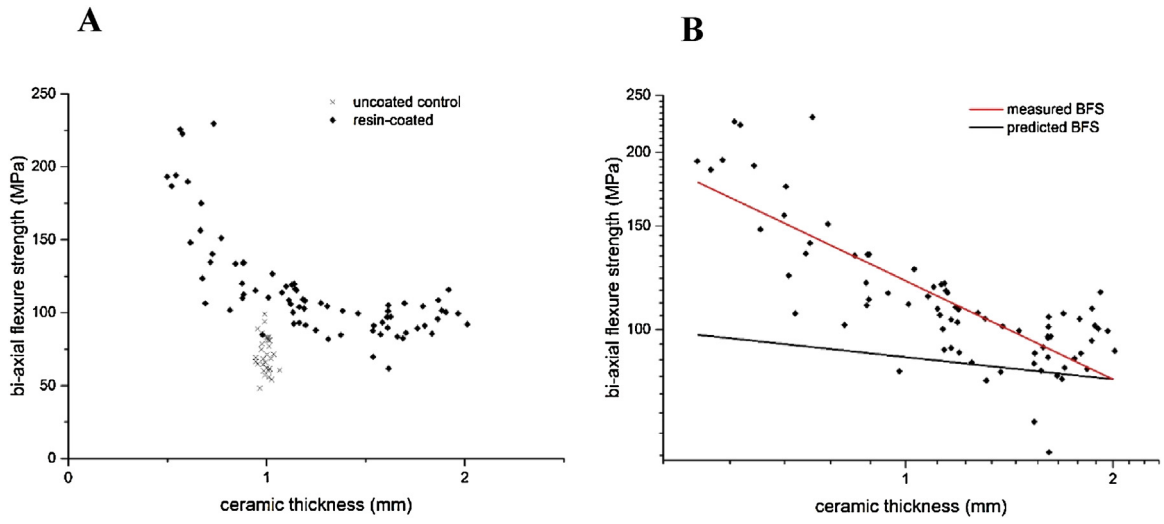

Fig. 3 – A) Scatter plot of ceramic thickness against BFS values measured 24 h following photo-polymerisation, and uncoated control data (specimens fabricated to 1 mm thickness) shown. B) Plot of measured BFS against ceramic thickness shown on logarithmic axes with trend-lines fitted to measured data and BFS predicted from Eq. (2.3), accounting for volume scaling effects, and referenced nominally to a sample of 2 mm thickness. The plot demonstrates that the measured BFS cannot be entirely accounted for by volume scaling effects shown by the predicted trendline.

4. Discussion

This study explores the link between shrinkage stresses associated with the photo-polymerisation of dental resin-based cements and the reinforcement of dental porcelain. Key variables to be considered when interpreting the measured data presented here include; the initial residual stress state of the disc-shaped specimens; the pre-existing, strength-limiting, ceramic surface defect population; the disc-flexural rigidity; the time following photo-polymerisation of the resin-cement; the nature of the resin-cement/ceramic adhesive interface and the impact of specimen thickness on strength-scaling.

The uncoated porcelain disc-shaped specimens were manufactured to represent a range of clinically relevant thicknesses ranging from 0.5 to 2 mm and therefore possessed differences in disc-flexural rigidity. Flexural rigidity is the reciprocal of compliance and relates to the ability of the disc-shaped specimen to resist deformation while in bending. At baseline (before photo-polymerisation), all specimens exhibited a convex curvature of the highly polished measurement surface. It has been suggested that this is due to the presence of a gradated residual stress field within the sample, with net relative tension in the upper polished surface relative to the lowermost surface [25,27], rather than 'form' which was introduced directly by the polishing regime. When specimens of different thicknesses (and therefore volume) are sintered, differences in thermally induced transient and residual stresses consequent to cooling will inevitably result [33], and this was exacerbated by one surface being in contact with the silicon nitride firing slab [24]. To account for the differences in the thermally induced transient and residual stresses consequent to cooling, all specimens were ground on both surfaces [27] and annealed [26]. Subsequently one surface was randomly chosen for further polishing and the other for alumina particle air abrasion. The fact that all specimens exhibited a convex baseline surface profile suggests that polishing was the dominant contributor to an initial tensile stress state existing over the polished measurement surface and is in accordance with previous reports [25,27]. Alumina particle air abrasion has been demonstrated to introduce both a consistent defect population on the surface of similar substrates [30] and residual tensile stresses as a consequence of surface and sub-surface damage [27]. Although baseline transient and residual stresses were not empirically measured, it was safe to assume consistency in the nature of residual stresses at baseline. Accepting the presence of pre-existing residual stresses, surface deformation was non-linearly associated with disc-flexural rigidity and the most compliant specimens possessed the highest mean baseline deflections. The non-linearity of this relationship can be accounted for by considering that in thinner (more compliant) discs, the proportion of the specimen volume under the non-homogeneous tensile residual stress is greater. With increasing ceramic thickness, the disc compliance reduces, determined by its elastic constants and the cube of its thickness Eq. (1.6) [31] (Fig. 1).

Resin-coating and photo-polymerisation resulted in a modification to the mean of the maximum deflection values (δ_{1440}-$\delta_{baseline}$) with two patterns of behavior observed. Thinner discs (approximately <0.7 mm) had increased mean of the maximum deflection values, and thicker discs (>0.7 mm) either showed no change or demonstrated a reduction in the mean of the maximum deflection values. Assuming that the interaction between the resin-cement/ceramic adhesive interface was equivalent for all specimens and that the magnitude of shrinkage stresses generated by photo-polymerisation of the resin-cement were consistent then three scenarios can be considered. Firstly, for the most compliant specimens the volumetric shrinkage of the resin-cement generates a compressive stress at the interface (and assuming they are interpenetrated, within the ceramic surface defects themselves). The compressive stress is accommodated for by the elastic tensile strain above the neutral axis of bending in the disc and is manifest as an increase in the deflection values (δ_{1440}-$\delta_{baseline}$) observed in the thinner (more compliant) discs. Secondly, shrinkages stresses are similarly generated but the disc-flexural rigidity (D) is too high to manifest as significant disc-deformation and in such cases the resin-cement would meet resistance to volumetric shrinkage. In this scenario the resin-cement/ceramic interface remains intimately intact and viscoelastic deformation within the resin-coating is not significant. Accordingly, any reduction in the mean of the maximum deflection values (δ_{1440}-$\delta_{baseline}$) may occur only if residual stresses are relieved at the reference ceramic surface by micro-crack generation. Thirdly, strain generated within the resin-cement as a result of disc-flexural rigidity results in regional losses of adhesion at the resin-cement/ceramic adhesive interface and, or viscoelastic deformation within the resin-cement. In such instances, stress relief would occur primarily within or be related to the resin-cement and no change in the mean of the maximum deflection values would be observed.

Statistically significant changes in the mean of the maximum deflection value were observed for all time points up until 90 min following photo-polymerisation. During resin photo-polymerisation, the gelation point and subsequent generation of shrinkage stresses is reached rapidly, followed by a much slower diffusion limited (post-cure) setting reaction [34]. The stabilisation of the changes in the mean of the maximum deflection value after 90 min points to a consistency in the net residual stress state throughout the specimen volume. The experimental methods used do not provide the sensitivity required to detect many of the phenomena that are expected to be occurring. However, it is likely that a range of events including stress relaxation within the resin-cement, at the resin-cement/ceramic interface and, or at the ceramic surface occur in response to the applied residual stress.

At 24 h following photo-polymerisation, BFS values were determined and increasing BFS values were strongly correlated with an increased vector of change in mean of the maximum deflection observed (δ_{1440}-$\delta_{baseline}$). However, while the current BFS values (115 ± 35 MPa) significantly exceeded the mean BFS values for the uncoated state (72 ± 9 MPa), low BFS values in the current study were clustered between 80–110 MPa which suggested a failure of reinforcement occurred for these specimens. Notably it was these low BFS value specimens clustered between 80–110 MPa which exhibited the smallest change (δ_{1440}-$\delta_{baseline}$) in the mean of the maximum deflections observed.

When considering the differences in BFS of resin-cemented specimens of different thicknesses, the effect of volume-scaling on ceramic strength, must be considered. With decreasing specimen volume, the statistical likelihood of encountering a strength limiting defect decreases and consequently the measured mean strength increases. The effective area and volume under stress during BFS testing in a ball-on-ring configuration, can be determined using the approach described by Frandsen [35] and used to model the influence of volume on the measured BFS. The modelling approach of Frandsen [35] requires an assumption that the BFS data adequately fits the Weibull distribution which is accepted as a limitation. The effective area (A_0) and effective volume (V_0) of the disc-shaped specimen loaded in a ball-on-ring configuration under an assumption of plane stress is described by Eqs. (2.1) and (2.2):

$$A_0 = \frac{R^2}{\left(\sigma^S_{max}\right)^m}\int_0^1 2\pi\rho\left[\left(\sigma^S_1\right)^m + \left(\sigma^S_2\right)^m\right]d\rho = 2\pi R^2\sum_{\gamma=1}^{2}\sum_{\Omega=I}^{III}J_{\Omega\alpha} \tag{2.1}$$

$$V_0 = \frac{h}{2(m+1)}A_0 \tag{2.2}$$

where m is the Weibull modulus, h is the plate thickness and equal to $t_1 + t_2$, σ^S refers to respective stress terms computed at the plate surface, ρ is the ratio of radial position to outer plate radius, and $J_{\Omega\alpha}$ are a series of dimensionless integrals. The computation of the $J_{\Omega\alpha}$ integrals includes terms such as the Poisson's ratio and other geometric factors, but is independent of plate thickness. Therefore, A_0 under a plane stress is independent of h whilst V_0 is linearly proportional to h.

Fractographic analysis identified the fracture origin in all resin-coated disc-shaped specimens evaluated in this study to originate from the ceramic surface. As A_0 is independent of h, altering the specimen thickness should not result in a change of effective area and therefore should not influence BFS. However, the critical surface defects extend to a variable length into the ceramic bulk and V_0 may therefore be relevant since a linear increase in V_0 occurs with increasing disc thickness. Using Eqs. (2.2) and (2.3) the relationship between the predicted scaled characteristic strength ($\sigma_{o'}$), the empirically determined characteristic strength (σ_o) and the changes in plate thickness (h) can be considered.

$$\left(\frac{\sigma_o{}'}{\sigma_o}\right)^m = \left(\frac{V_o}{V_o{}'}\right) \tag{2.3}$$

$V_{o'}$ the scaled effective volume, reduces linearly with decreasing h, for an arbitrary constant A_0. Referencing σ_o for a 2 mm thick specimen, the contribution of strength scaling to the observed increase in mean BFS value for 1.0 and 0.5 mm thickness disc-shaped specimens was 18% and 23% of the measured reinforcement, respectively (Fig. 3B) for $m = 5.6$ (where m was calculated from the fracture strength data of this study).

Whilst it is clear that volume-scaling effects do not account for the majority of the observed behavior, it is unlikely that the magnitude of strengthening observed can be accounted for entirely by crack-closure stress caused by shrinkage of the resin-cement. More complex phenomena such as enhancement of crack-tip shielding by sample deformation, should be considered. The current study provides some insight into a complex interaction between resin-cement and ceramic surface defects. The implication of the findings is that it is possible (at least initially) to generate residual stress states which can impact upon the strength of a 'weak' dental porcelain. Medium and long term exposure to the oral environment will introduce effects of water sorption and hydrolysis (both of the resin-cement and its interface with the ceramic) which are likely to alter the observed behavior. The study also isolated one interface and the impact of restricting resin-cement volume and altering further system compliance through adhesion to the underlying substrate has yet to be considered, and is likely to modify the observed patterns of behavior further.

Acknowledgement

This study was funded by the Engineering and Physical Sciences Research Council UK grant code EP/H028617/1.

REFERENCES

[1] Burke FJT, Fleming GJP, Nathanson D, Marquis PM. Are adhesive technologies needed to support ceramics? An assessment of the current evidence. J Adhes Dent 2002;4:7–22.
[2] van Dijken JW, Höglund-Aberg C, Olofsson AL. Fired ceramic inlays: a 6-year follow up. J Dent 1998;26:219–25.
[3] Malament KA, Socransky SS. Survival of Dicor glass-ceramic dental restorations over 14 years: Part 1. Survival of Dicor complete coverage restorations and effect of internal surface acid etching, tooth position, gender and age. J Prosthet Dent 1999;81:23–32.
[4] Scherrer SS, de Rijk WG. The fracture resistance of all-ceramic crowns on supporting structures with different elastic moduli. Int J Prosthodont 1993;6:462–7.
[5] Burke FJ, Watts DC. Effect of differing resin luting systems on fracture resistance of teeth restored with dentin-bonded crowns. Quintessence Int 1998;1998(29):21–7.
[6] Tinschert J, Natt G, Mautsch W, Augthun M, Spiekermann H. Fracture resistance of lithium disilicate-, alumina-, and zirconia-based three-unit fixed partial dentures: a laboratory study. Int J Prosthodont 2001;14:231–8.
[7] Attia A, Kern M. Fracture strength of all-ceramic crowns luted using two bonding methods. J Prosthet Dent 2004;91(3):247–52.
[8] Borges GA, Caldas D, Taskonak B, Yan J, Sobrinho LC, de Oliveira WJ. Fracture loads of all-ceramic crowns under wet and dry fatigue conditions. J Prosthodont 2009;18:649–55.
[9] Kelly JR, Benetti P, Rungruanganunt P, Bona AD. The slippery slope: critical perspectives on in vitro research methodologies. Dent Mater 2012;28:41–51.
[10] Kikuchi M, Korioth TW, Hannam AG. The association among occlusal contacts, clenching effort, and bite force distribution in man. J Dent Res 1997;76:1316–25.
[11] Qasim T, Ford C, Bush MB, Hu X, Malament KA, Lawn BR. Margin failures in brittle dome structures: relevance to

failure of dental crowns. J Biomed Mater Res B Appl Biomater 2007;80:78–85.
[12] McLean JW. Ceramics in clinical dentistry. Br Dent J 1988;164:187–94.
[13] Denry I, Kelly JR. Emerging ceramic-based materials for dentistry. J Dent Res 2014;93:1235–42.
[14] Lawn BR, Deng Y, Miranda P, Pajeres A, Chai H, Kim DK. Overview damage in brittle layer structures from concentrated loads. J Mater Res 2002;17:3019–36.
[15] Rekow D, Thompson VP. Engineering long term clinical success of advanced ceramic prostheses. J Mater Sci Mater Med 2007;18:47–56.
[16] Kelly JR, Benetti P. Ceramic materials in dentistry: historical evolution and current practice. Aust Dent J 2011;56:84–96.
[17] May LG, Kelly JR, Bottino MA, Hill T. Effects of cement thickness and bonding on the failure loads of CAD/CAM ceramic crowns: multi-physics FEA modeling and monotonic testing. Dent Mater 2012;28:99–109.
[18] Zhang Y, Sailer I, Lawn BR. Fatigue of dental ceramics. J Dent 2013;41:1135–47.
[19] Fleming GJP, Maguire RF, Bhamra G, Burke FM, Marquis PM. The strengthening mechanism of resin cements on porcelain surfaces. J Dent Res 2006;85:272–6.
[20] Addison O, Marquis PM, Fleming GJP. Resin strengthening of dental ceramics—the impact of surface texture and silane. J Dent 2007;35:416–24.
[21] Addison O, Marquis PM, Fleming GJP. Resin elasticity and the strengthening of all-ceramic restorations. J Dent Res 2007;86:519–23.
[22] Nathanson D. Principles of porcelain use as an inlay/onlay material. In: Gaber GA, Goldstein RE, editors. Porcelain and composite inlays and onlays. Illinois: Quintessence; 1993. p. 23–32.
[23] Kelly RD, Fleming GJP, Hooi P, Palin WM, Addison O. Biaxial flexure strength determination of endodontically accessed ceramic restorations. Dent Mater 2014;30:902–9.
[24] Fleming GJP, Shaini FJ, Marquis PM. An assessment of the influence of mixing induced variability on the bi-axial flexure strength of dentine porcelain discs and the implications for laboratory testing of porcelain specimens. Dent Mater 2000;16:114–9.
[25] Isgró G, Addison O, Fleming GJP. Deformation of a dental ceramic following adhesive cementation. J Dent Res 2012;89:87–90.
[26] Denry IL, Holloway JA, Tarr LA. Effect of heat treatment on microcrack healing behavior of a machinable dental ceramic. J Biomed Mater Res 1999;48:791–6.
[27] Isgró G, Addison O, Fleming GJP. Transient and residual stresses induced during the sintering of two dentin ceramics. Dent Mater 2011;27:379–85.
[28] Hsueh CH, Lance MJ, Ferber MK. Stress distributions in thin bilayer discs subjected to ball-on-ring tests. J Am Ceram Soc 2005;88:1687–90.
[29] Borba M, de Araújo MD, de Lima E, Yoshimura HN, Cesar PF, Griggs JA, Della Bona A. Flexural strength and failure modes of layered ceramic structures. Dent Mater 2011;27:1259–66.
[30] Addison O, Marquis PM, Fleming GJP. Quantifying the strength of a resin-coated dental ceramic. J Dent Res 2008;87:542–7.
[31] Young WC, Budynas RG. Chapter 11, flat plates. In: Young WC, Budynas RG, editors. Roark's formulas for stress and strain. 7th edition New York: McGraw-Hill; 2002. p. 427–525.
[32] Geisser S, Greenhouse SW. An extension of Box's result on the use of F-distribution in multivariate analysis. Ann Math Statist 1958;29:885–91.
[33] Coffey JP, Anusavice KJ, DeHoff PH, Lee RB, Hojjatie B. Influence of contraction mismatch and cooling rate on flexural failure of PFM systems. J Dent Res 1988;67:61–5.
[34] Halvorson RH, Erickson RL, Davidson CL. Energy dependent polymerization of resin-based composite. Dent Mater 2002;18:463–9.
[35] Frandsen HL. Weibull statistics effective area and volume in the ball-on-ring testing method. Mech Mater 2014;73:28–37.